Research Article

Published in Cardiovascular Engineering and Technology.
Full reference: Ngoepe MN, Reddy BD, Kahn D, Meyer C, Zilla P, Franz T. A numerical tool for the coupled mechanical assessment of anastomoses of PTFE arterio-venous access grafts. Cardiovasc Eng Tech, 2011, 2(3), 160-72

A Numerical Tool for the Coupled Mechanical Assessment of Anastomoses of PTFE Arterio-venous Access Grafts

M. N. Ngoepe[1], B. D. Reddy[1], D. Kahn[2], C. Meyer[1], P. Zilla[3], T. Franz[1,3]*

[1]Centre for Research in Computational and Applied Mechanics, University of Cape Town, Private Bag, Rondebosch 7701, South Africa

[2]Transplant Unit & Division of General Surgery, University of Cape Town, Private Bag X3, Observatory 7935, South Africa

[3]Chris Barnard Division of Cardiothoracic Surgery, University of Cape Town, Private Bag X3, Observatory 7935, South Africa

* Send correspondence to:

Thomas Franz, PhD

Cardiovascular Research Unit

Faculty of Health Sciences

University of Cape Town

Private Bag X3, Observatory 7935, South Africa

Tel.: +27 21 406 6410; Fax: +27 21 448 5935

Email: Thomas.Franz@uct.ac.za

ABSTRACT

Purpose: The anastomotic angle is assumed to affect the performance of arterio-venous (AV) access grafts by altering wall shear stress (WSS) and wall tension. The objective of this study was to develop a coupled numerical tool to assess fluid and structural anastomotic mechanics of a straight upper arm access graft.

Methods: 3D computational fluid dynamics (CFD) and finite element (FE) models were developed for arterial and venous anastomoses with different graft attachment angles. The fluid simulations were executed using flow velocity profiles for anastomotic inlets obtained from a whole-graft CFD model. A mesh adaptation algorithm was developed to couple CFD and FE meshes and capture fluid structure interactions.

Results: The coupling algorithm enabled transfer of blood pressure (BP) and WSS predicted with the CFD models to the FE models as loadings. The deformations induced in the FE models were used to update the CFD geometries after which BP and WSS were recalculated and the process repeated until equilibrium between fluid and solid models. Maximum BP in the vein was 181 mmHg. WSS peaked at 2.3 and 0.7 Pa and the structural wall stress reached 3.38 and 3.36 kPa in arterial and venous anastomosis.

Conclusions: Since flow-induced wall tension has been identified as a contributor to access graft failure along with WSS, the computational tool will be useful in studying the coupled mechanics in these grafts. Initial investigations of arterial and venous anastomotic end-to-side configuration indicated a slightly better performance of the 90° configuration over 135° arterial and 45° venous configurations.

Keywords: Arterio-venous access; Haemodialysis; Finite element method; Computational fluid dynamics; Fluid structure interaction

1. INTRODUCTION

Patients undergoing haemodialysis require vascular access to ensure that blood leaves the body and enters the dialysis machine at a sufficiently high flow rate of 300 – 500 ml/min or greater.[28] The three commonest forms of vascular access are arterio-venous (AV) fistulae, AV grafts and tunnelled catheters. The AV fistula, formed by joining the patient's native artery to the native vein, is the preferred form of access.[43] In cases where it is not possible to create an AV fistula, an AV graft is inserted by using an artificial graft to connect the artery and the vein. Catheters are used when neither the fistula nor the graft can be used.

There are various configurations of the AV grafts. These include the forearm loop graft, the upper arm straight graft, upper arm loop graft and the thigh graft. Of particular interest is the upper arm straight graft, where a graft is used to join the brachial artery to the axillary vein. For this particular configuration, surgeons facilitate different connection angles when joining the artificial graft to the native vessels. It is possible that the connection angle has an effect on the local hemodynamics in the anastomotic region and thus on graft patency; however it is not known which angle has more benefits. Several factors have been identified as causes of AV graft failure. Mechanical factors which are perceived as major contributors to neointimal hyperplasia development and subsequent graft failure include trauma of the native vessel walls from suturing and material mismatch between the artificial PTFE grafts and the native vessel wall.[1, 4] Hemodynamic factors viewed as triggers of neointimal hyperplasia include low fluid shear stress and increased wall stress.[28, 24] For PTFE AV grafts, patency rates as low as 40% after four years have been reported,[8] with straight grafts performing poorer than loop grafts.[41]

The use of computational methods has been reported for the study of hemodynamics in vascular access for haemodialysis, focussing primarily anastomotic regions. Loth at al.[27] combined computational fluid dynamics (CFD) with ultrasound Doppler measurements in patients to investigate the link between hemodynamics and the development of intimal hyperplasia in venous anastomotic

regions of PTFE AV grafts. The potential role of transitional blood flow and vein wall vibration in the failure of AV grafts was investigated computationally using a spectral element method.[23, 22] While velocity and pressure fluctuations measured in vivo[23] were present in the numerical simulations, their magnitude and frequency did not correlate well with the in vivo results of vein wall vibration obtained with laser Doppler vibrometry. Van Tricht et al.[42] used CFD to compare the hemodynamics in a straight and tapered AV graft. Kharboutly et al.[16, 15] conducted patient-specific CFD simulations and in vivo experiments to investigate the fluid mechanics in an AV fistula and the role of flow pattern in pathological alterations of the vascular wall. CFD has also been employed to investigate anastomotic regions of bypass grafts.[5, 26, 39, 4, 32] Although these studies were motivated similarly by pathological responses observed in particular at the distal anastomosis of arterial bypass grafts, the simulations focussed at arterial blood flow; as such they did not deal with the fluid mechanics of AV connections.

The objective of this study was to develop a coupled numerical tool for the assessment of both fluid mechanics of the blood and solid mechanics of the vascular conduits of upper arm straight PTFE access grafts. A three-dimensional (3D) CFD model of a simplified artery-graft-vein configuration was used to simulate the fluid dynamics over entire length of the graft and similar lengths of artery and vein. Subsequently, 3D CFD models and finite element (FE) models were developed for two different geometrical configurations of the arterial and venous anastomotic regions. In order to capture the mechanical interaction between blood and blood vessel, the FE models, representing the arterial and venous tissue and the PTFE graft, were linked to the CFD models using a custom coupling algorithm.

2. METHODS

2.1 Anastomotic geometries

Two geometrical variations of the arterial and venous anastomotic region, respectively, were considered. The arterial anastomosis was modelled with an angle of change in blood flow direction, β,

from the artery into the graft of β = 90° and 135° (as illustrated in Fig. 1). The venous anastomosis was modelled with change in blood flow direction from the graft into the vein of β = 45° and 90° respectively. Artery, vein and PTFE graft were represented with simplified cylindrical geometries with inner and outer diameters summarised in Table 1. The artery had greater wall thickness than the PTFE graft, thus the two intersecting cylinders were not equal in inner diameter. In order to compensate for this, the geometry of the artery was tapered from the correct thickness at the outer ends to a thickness equal to that of the PTFE graft at the point where the two cylinders intersected at the anastomosis. This was valid because suturing of the graft to the artery would have this effect on the anastomotic region and is illustrated in Fig. 1(a). The vein and graft dimension were identical thus it was not necessary to taper the cylinders at any point. The geometry therefore comprised two cylinders intersecting at the required angle as seen in Fig. 1(b).

2.2 Material models

Native blood vessels

The arteries and veins were modelled as non-linear elastic materials with the stress-strain relationship being described using a strain energy function. A constitutive framework for the realistic description of blood vessel walls developed by Holzapfel et al[13] was used to describe the behaviour of the media and adventitia layers of each vessel. The intima can be neglected since the contribution of this layer to the solid mechanical properties is sufficient small.[13] The strain energy function is given by

$$\overline{\psi_L} = \frac{C_L}{2}(\overline{I_1} - 3) + \frac{k_{1L}}{2k_{2L}} \sum_{i=4,6} \{exp[k_{2L}(\bar{I}_{iL} - 1)^2] - 1\} \quad (1)$$

where L is the layer of interest (either the adventitia or the media), C is a constant relating to the non-collagenous matrix of the vessel wall and k_1 and k_2 are constants relating to the collagenous fibres of the vessel wall. I_1 is the first invariant of the modified Cauchy-Green tensor, $\bar{C}$, with

$$\bar{I}_1 = tr\bar{C} = \sum_{i=1}^{3} \lambda_i^2 \quad (2)$$

where λ is the principal stretch, the ratio of the fibre's deformed length to the original length in the ith direction. The model, initially developed for the arterial wall, models the artery wall as a two-layer, thick, non-linear elastic cylinder. Each layer is modelled as a fibre-reinforced material with the fibres representing the collagen in the real artery wall. The constitutive parameters used for the media and adventitia of artery and vein[3], respectively, are summarised in Table 2. The model assumes that the artery is stress free when it is modelled as an open sector of a tube but that when found in its natural closed state, it has residual stresses, thus making it load free but not stress free.[13]

PTFE graft

The PTFE graft material was modelled as a non-linear elastic material. The Ogden model,[33] which accurately describes the behaviour of rubberlike materials over a large range of deformations, was used to describe the behaviour of the graft. The model's strain energy function is expressed in terms of principal stretches and is given by

$$U = \sum_{i=1}^{N} \frac{2\mu_i}{\alpha_i^2}\left(\bar{\lambda}_1^{\alpha_i} + \bar{\lambda}_2^{\alpha_i} + \bar{\lambda}_3^{\alpha_i} - 3\right) + \sum_{i=1}^{N} \frac{1}{D_i}(J^{e\ell} - 1)^{2i} \quad (3)$$

where N is a material property, μ_i, α_i and D_i are temperature dependant material properties, $\bar{\lambda}$ are the deviatoric principal stretches $\bar{\lambda_i} = J^{-\frac{1}{3}}\lambda_i$ and λ_i are principal stretches[10]. The following material parameters were used[25]: μ_1 = -195.0 MPa, μ_2 = 405.0 MPa, μ_3 = 191.0 MPa, α_1 = 2.0, α_2 = 4.0, α_3 = -2.0.

Suture

The Prolene® suture was modelled as a homogenous, linear elastic, orthotropic material. For orthotropic mechanical properties, there are two perpendicular symmetry planes at any given point in

the material.[10] The material is defined by the elastic modulus, E, (ratio of stress to strain), the shear modulus, G (ratio of shear stress to shear strain) and Poisson's ratio, ν (ratio of lateral to longitudinal strain) for the axial (a), radial (r) and circumferential (c) material direction[1, 18, 37]: E_a = 969 kPa, E_r = 97 kPa, E_c = 97 kPa, G_a = 325 kPa, G_r = 33 kPa, G_c = 33 kPa and ν = 0.49.

Blood

Blood was modelled as a Newtonian, homogenous fluid with a density[36] of ρ = 1050 kg/m^3 and constant viscosity[21] of μ = 0.0032 kg/ms. The assumption of Newtonian behaviour were considered valid since the diameters of the vessels were considered sufficiently large.[7]

2.3 Computational fluid dynamics models

One complete fluid model which included the artery, graft and vein was developed (GAMBIT®, Ansys, Canonsburg, PA, USA) in order to obtain an approximation of the flow behaviour through a simplified configuration of an upper arm straight AV graft from the brachial artery at elbow level to the axillary vein in the axillia at different stages of the cardiac cycle. In addition, four fluid meshes were developed (GAMBIT®) for the arterial and venous anastomotic region utilising the geometries describe in Section 2.1. Individual fluid meshes were required to obtain compatibility of the common boundary with the solid (finite element) meshes for each anastomotic configuration.

Velocity boundary conditions were used for all inlets of the complete and anastomotic models. For arterial inlets, the inlet velocity profile for the artery was assumed to be pulsatile.[34]. The velocity wave form of one full cardiac cycle with a duration of 1.0s (representing a heart rate of 60 bpm), illustrated in Fig. 2, was discretized into 1000 steps.

The values of the pulsatile waveform for the graft inlet of the venous anastomotic models were obtained from the complete fluid model at the respective location. Steady flow across the diameter with a flow rate of 40 ml/min was assumed for the vein inlet[11, 12] of the complete model and the venous anastomotic models. All inlet velocity profiles were parabolic as it was assumed that flow was fully developed.

Simulations were performed in FLUENT® 12 (Ansys, Canonsburg, PA, USA) using the SIMPLEC algorithm (Semi-Implicit Method for Pressure-Linked Equations, Consistent)[40] to solve the Navier Stokes and continuity equations. The SIMPLEC algorithm is an extension of the well-established SIMPLER (Semi-Implicit Method for Pressure-Linked Equations) algorithm for solving the Navier-Stokes equations (that is, the momentum and continuity equations) iteratively for the velocity and pressure. The SIMPLEC algorithm differs from SIMPLER through the addition of a further consistent pressure correction. Flow velocity of the blood, luminal pressure and wall shear stress were used as output parameters of the fluid models.

2.4 Finite element models

ABAQUS® (Dassault Systemes, Providence, RI, USA) was used to develop the solid meshes of the arterial and venous anastomotic geometries to complement the fluid meshed describe above. Eight-node, linear brick hybrid (C3D8H) elements were used for the solid domain. These were chosen as they were suitable for all the material models employed. Each mesh consists of approximately 14097 nodes and 14059 elements. As boundary conditions in the arterial anastomosis models, the outlet of the artery was fully fixed, preventing movement in axial and radial direction. The artery inlet and graft outlet were fixed in axial direction only, allowing movement in radial direction. For the venous anastomoses, the vein outlet was fully fixed whereas the inlets of vein and graft were fixed axially but not radially.

Fluid pressure and wall shear stress obtained from the relevant fluid models were applied as loads to each of the solid models. In order to compare the various FEM model and solid anastomotic geometries, respectively, the maximum principal stress and the radial deformation of the vascular wall were utilised. The maximum principal stress is the largest of three principal stresses (for the three-dimensional case) each of which acts normal to one of the three principal planes in a solid for which the shear stress is zero. The maximum principal stress is as such the largest stress acting in a solid.

2.5 Fluid structure interaction

The fluid structure interaction code was written in MATLAB® (MathWorks, Natick, MA, USA) and allowed for coupling of the solid and fluid meshes, which were compatible at the common boundary. The principal steps followed in the code are listed below while a schematic representation is given in Fig. 3.

1. The first FLUENT® blood flow simulation was run and the pressure and shear stress results for each element was obtained
2. The pressure and shear stresses were applied to the respective solid elements in the ABAQUS® input file and the ABAQUS® simulation was run.
3. The displacements were obtained from the results of the ABAQUS® simulation and these were used to adapt the common boundary for both the solid and the fluid meshes.
4. A FLUENT® blood flow simulation was run based on the adapted mesh and pressure and shear stress results were obtained again.
5. The iterative process was repeated until convergence was reached.

3. RESULTS

3.1 Flow velocity

Figure 4(a) illustrates the flow velocity contours for the 135° arterial anastomosis model for time t = 1.0 s (see Fig. 2). A maximum velocity value of 0.24 m/s was observed at the artery inlet while a recirculation zone was seen in the graft close to the anastomosis. The velocity in this zone was zero. In the 90° arterial anastomosis model, the maximum flow velocity in the artery inlet was also 0.24 m/s and a similar recirculation zone was present, see in Fig. 4(b). The effects of the recirculation zone were less prominent on the flow in the rest of the graft for the 90° model compared to the 135° configuration. Figure 4(c) illustrates the flow velocity contours for the 45° venous anastomosis model. The maximum flow velocity for this model was 0.0886 m/s at the vein outlet while Fig. 4(d) shows that a maximum flow velocity of 0.0847 m/s was reached at the vein outlet for the 90° venous

anastomosis model. There was no evidence of recirculation zones in either of the venous anastomosis models.

3.2 Wall shear stress

The shear stress pattern varied over the entire wall surface of the 135° arterial anastomotic region, as seen in Fig. 5(a) at t = 1.0 s (see Fig. 2). A maximum shear stress value of 2.32 Pa was observed at the anastomosis while the minimum shear stress regions were observed on the artery floor opposite the graft and at the recirculation zone described in the velocity results. Figure 5(b) displays a maximum shear stress value of 2.16 Pa at the anastomosis of the artery-graft 90° model while minimum shear stress regions were observed at the same sites as for the 135° model. The diagram also illustrates greatly varying shear stress over the entire wall surface. The maximum shear stress for the 45° graft-vein model was observed at the anastomosis with a value of 0.569 Pa as seen in Fig. 5(c). The minimum shear stress was observed over most of the graft wall. Figure 5(d) illustrates the shear stress contours for the vein 90° model where a maximum shear stress value of 0.702 Pa was predicted. The shear stress varied less over the entire wall surface for the vein models when compared to the artery models.

3.3 Luminal Pressure

Figure 6(a) illustrates a maximum pressure of 16.70 Pa (125.3 mmHg) at time t = 1.0 s (see Fig. 2) for the 135° artery-graft model on the distal side of the anastomosis. A relatively high pressure zone was observed at the anastomotic toe and in the artery downstream of the bifurcation while the pressure was lower in the graft and the artery upstream of the anastomosis. A minimum pressure of -4.30 Pa (-32.3 mmHg) was observed in the heel of the anastomosis . Similar patterns were observed in the 90° artery-graft model (see Fig. 6(b)), with a maximum pressure of 14.00 Pa (105.0 mmHg) predicted at the anastomotic toe and a minimum pressure of -4.04 Pa (-30.3 mmHg) observed in the anastomotic heel. The pressure distribution in the venous anastomotic models was somewhat different with the pressure decreasing gradually from a maximum value of 24.20 Pa (181.5 mmHg) at the vein inlet to a minimum value of 1.21 Pa (9.1 mmHg), as seen in Fig. 6(c), for the 45° venous anastomosis. A similar pattern was noticed in Fig. 6(d) for the 90° venous anastomosis model where the pressure

decreased from a maximum value of 14.40 Pa (108.0 mmHg) at the vein inlet to 0.72 Pa (5.4 mmHg) at the vein outlet.

3.4 Maximum principal stress in the vascular wall

Figure 7(a) illustrates the maximum principal stress at t = 1.0 s (see Fig. 2) for the 135° artery-graft anastomosis, with a maximum value of 3.38 kPa observed at the anastomosis. The maximum principal stress in the graft was fairly uniform and varied over the artery wall, where higher stresses were observed close to the artery inlet. The maximum principal stress in the 90° arterial anastomotic model also reached a maximum at the anastomosis, in this case with a value of 1.39 kPa. This is illustrated in Fig. 7(b), which also depicts a fairly constant stress over the graft wall and varying stress over the artery wall. Figure 7(c) depicts the maximum principal stress for the 45° venous anastomosis model, with constant stress over the vein wall and varying stress over the graft wall. The maximum stress observed for this model was 3.36 kPa while that for the 90° venous anastomosis model was 1.71 kPa as seen in Fig. 7(d). The stress was fairly constant over both the graft and vein walls for the 90° venous anastomosis and the maximum stress is observed at the anastomosis for both models.

3.5 Radial deformation of the vascular wall

Figure 8(a) depicts the magnitude of the radial deformation for the 135° artery-graft anastomotic model at t = 1.0 s (see Fig. 2). A maximum deformation value of 6.46 mm was observed in the region of the artery inlet whereas the minimum deformation occurred at the artery outlet. A similar trend was evident in the 90° arterial anastomosis (Fig. 8(b)), which had a maximum deformation value of 3.71 mm. Figure 8(c) illustrates the deformation magnitude plot for the 45° graft-vein anastomosis with a maximum deformation of 0.48 mm. For both the 45° and the 90° venous anastomotic model, the maximum and minimum deformation was observed at the vein inlet and outlet, respectively. The maximum deformation for the 90° model, seen in Fig. 8(d), was 0.33mm mm.

4. DISCUSSION

In this study, we developed a tool for the coupled three-dimensional simulation of the hemodynamics and structural mechanics of the blood vessels for arterio-venous access grafts. The computational tool comprised computational fluid dynamics models, finite element models and a fluid structure interaction algorithm. While CFD and FE models were implemented in commercial software packages, the 3D fluid structure interaction code was developed in house based on an algorithm for two-dimensional coupling of fluid and structural domains based on a grid-adaptation algorithm.[37] The grid adaptation algorithm was used to adjust the nodal coordinates of the fluid domain to match the nodal coordinates of the solid mesh in each solution iteration. This ensured that fine mesh details were maintained during geometric adaptation of the fluid domain. New nodal coordinates for the common wall boundary nodes were accommodated in the fluid domain by interpolative adjustment of the radial coordinates of internal nodes while axial coordinates of the nodes were retained. A simplified CFD model of the entire graft was employed to obtain approximations for the flow boundary conditions in the anastomotic regions. These data were used in CFD models of the arterial and venous anastomoses. The pressure and wall shear stress predicted with the CFD models were transcribed to the respective FE models and, acting as loading, induced a deformation of the solid model. The deformed solid domain, representing the blood vessels, was subsequently implemented in the CFD models after which the fluid parameters, including pressure and wall shear stress, were updated. This process was repeated iteratively until equilibrium between fluid and solid models was achieved.

Compared to studying anastomotic mechanics of AV access graft with CFD alone, the fluid-structure coupled approach presented here provides additional information, i.e. deformations and stresses in vascular tissue and graft wall. With the prediction of flow pattern and wall shear stress,[27, 23, 22, 15, 16, 41] CFD allows the assessment of one important trigger of intimal hyperplasia. However, studies of vein grafts indicated that increased circumferential deformation and stress, respectively, in the vessel wall is an additional trigger of vein graft failure.[46, 6, 38] Since the venous anastomosis and the vein downstream of the AV graft have been reported as predominant failure,[14, 27] the consideration of structural parameters such as wall tension seems also to be important in the context of AV grafts. CFD models, limited to the fluid domain, cannot be used to assess structural parameters of the

vascular tissue and graft. By incorporating the solid structures as deformable bodies in the model, the couple method overcomes this limitation.

The flow contours in the vein and in the graft were parallel to each other as would be expected because a parabolic inlet flow velocity profiles were imposed for both. The flow velocity in the vein increased towards the outlet from the point where the graft and vein streams meet. The contour plots for the arterial anastomosis models were mostly normal with parallel streamlines observed close to the artery inlet. The flow pattern in the graft after the bifurcation was characterised by a recirculation zone in the graft towards the heel of the anastomosis. The recirculation zone was more developed and had a greater effect on the flow in the 135° arterial anastomosis, where the surrounding contours bulge out in a similar fashion up to the axis of the graft. This effect was less pronounced in the 90° model.

The wall shear stress patterns for the two venous anastomotic configurations were similar and depicted maximum shear stress in the toe region of the anastomosis. This agrees with results presented by Loth et al.[27] Lower shear stress values were observed at the graft wall for both models. The low shear stress values in the graft were probably caused by the different flow velocity profiles imposed at graft inlet compared to the vein inlet. In the vein, a gradual change in wall shear stress was predicted for both models; with values for the 45° model slightly lower than those of the 90° model. In the arterial anastomoses, the wall shear stress values varied greatly over the arterial wall. For both models, there was a low shear stress zone on the artery floor opposite the graft attachment and at the flow recirculation zone. The former coincided with the region where the flow splits, with some of the flow was moving towards the artery outlet and the remainder of the flow moving towards the graft outlet. As the recirculation zone was characterised by low flow velocity, lower shear stresses were a consequence.

The pressure contours for the two venous anastomoses were very similar. For both, maximum and minimum pressure was observed at the inlet and outlet, respectively, of the vein. In general, the pressure values were higher in the 45° anastomosis model than those of the 90° model with maxima

reaching 24-fold (45° model) and 14-fold (90° model) of venous pressure in the upper arm of 1 Pa (97 mmH_2O[44] = 7.1 mmHg) and 1.5-fold (45° model) and 0.9-fold (90° model) of arterial systolic pressure (16 Pa, 120 mmHg). The pressure contour plots for the artery models were also fairly similar. The pressure values were relatively low in the artery upstream of the bifurcation and in the graft. Higher pressure regions were observed in the artery at the inlet and downstream of the flow split. Maximum pressure values were predicted in the anastomotic toe. The minimum pressure was observed at the anastomotic heel where the negative pressure values in both models were ascribed to the flow recirculation in the graft. A negative luminal pressure in a larger region may cause the collapse of a blood vessel. Whether the predicted concentrated negative pressure regions reflect a physiological phenomenon or is caused by limitations of the models, e.g. the boundary conditions, needs to be further investigated in future studies.

The maximum principal stress contours indicated maximum stress values to occur at the anastomosis for the all anastomotic models. In the 45° venous anastomosis, the stress was fairly constant over the vein wall but varied in the graft wall. The heel region of the graft exhibited larger stresses than the hood region. For the 90° venous anastomosis, the stress was distributed more axisymmetrically in the graft wall but increased from graft inlet towards the anastomotic interface. While the maximum principal wall stress in the vein was constant from inlet to anastomosis, it increased downstream from the anastomosis towards the outlet. The stress at the suture line (anastomotic interface) was slightly lower than the stress experienced by either the graft or the vein due to the material properties of the suture. Overall, the 45° venous anastomosis exhibited a nearly two-fold (1.96) maximum principal stress compared to the 90° anastomosis. In the arterial anastomosis, the maximum principal wall stress was fairly uniform in the graft, except in vicinity of the anastomotic interface, but varied in the artery for both anastomotic configurations. Interestingly, the variation of wall stress in the artery was predominantly in circumferential direction with little changes observed longitudinally from artery inlet to outlet, for the 90° anastomosis. The 135° model, however, predicted stress variation both in circumferential and longitudinal direction, in particular from the artery inlet to the artery-graft

junction. Similarly to the observations for the venous anastomosis, the 90° arterial model predicted a lower maximum wall stress compared to 135° arterial anastomosis.

All four models depicted similar trends for the deformation magnitude, where the deformation was largest at the vessel inlet and gradually decreased to the smallest deformation at the vessel outlet. For the arterial and the venous anastomosis, smaller wall deformation was predicted in the 90° configuration reaching 57% and 69% of the wall deformation observed in the 135° arterial anastomosis and 45° venous anastomosis.

Summarising the findings of wall shear stress, luminal pressure, maximum principal wall stress and wall deformation, higher maximum values were predicted for all four parameters, at the end of the cardiac cycle (at t = 1.0 s, see Fig. 2), in the 135° arterial anastomosis compared to the 90° arterial anastomosis. While the difference was moderate for shear stress (1.1-fold) and luminal pressure (1.2-fold), the wall stress and deformation differed somewhat more pronounced between the two models (2.4-fold and 1.7-fold). This indicated that the 90° arterial anastomosis may be superior to the 135° attachment of graft to the artery. However, the latter showed a somewhat smaller blood flow recirculation zone in the heel region of the graft, despite the more severe change in blood flow direction. For the two venous anastomoses, the 45° graft attachment caused a lower maximum level of shear stress (0.8-fold) but higher maxima of luminal pressure (1.7-fold) and wall stress (2.0-fold) and wall deformation (1.5-fold) compared to the 90° grafts attachment. With low shear stress[31, 17] and high circumferential wall stress[19, 38] being causes of intimal hyperplasia, the 90° attachment seems to be preferable over the 45° degree attachment. However, while the maximum shear stress was different in the two models, the magnitudes of shear stress predicted in the vein did not support a firm conclusion whether intimal hyperplasia is to be expected in either anastomotic configuration. While the maximum shear stress was 0.57 and 0.70 Pa (45° and 90° model), the shear stress level in the vein was in the region of 0.2 – 0.3 Pa (Fig. 5 c and d). While these values exceeded the shear stress threshold of 0.1 Pa for intimal hyperplasia in the venous circulation,[35] they fell short of the shear stress of 0.5 Pa below which intimal hyperplasia is triggered in vein grafts in arterial circulation.[45] The

arterio-venous connection represents a transition between arterial and venous circulation not only with regard to shear stress and flow velocity but also in terms of luminal pressure and resulting tissue deformations. While the vein dilates during several weeks after AV graft construction,[9] the spontaneous dilation of veins when exposed to elevated luminal pressure has been reported to be limited. Martinez et al. observed for canine jugular veins the arrest of dilation at a circumferential stretch ratio of circa 1.2, i.e. 20% dilation, reached at a pressure of 20 mmHg.[29] The limited spontaneous dilation agreed with the current study which did not predict a pronounced dilation of the vein although the luminal pressure increased to 24.2 Pa (181 mmHg) and 14.4 Pa (108 mmHg), respectively, at the vein inlet.

This initial study focussed primarily at the establishment of the coupled numerical method. Some aspects, such as the simplified representation of the vascular and anastomotic geometries, will need more attention in future refined studies. This also applies to the evaluation of flow and structural parameters throughout the cardiac cycle whereas this study presented a snapshot at the end of the cardiac cycle.

CONCLUSIONS

The established computational tool allows for the assessment of fluid mechanics and structural mechanics, as well as the interaction between both, in arterio-venous access grafts and their anastomotic configuration. Since flow-induced structural deformation of the native blood vessels, in particular the vein, has been identified as a potential contributor to AV access graft failure, the fluid-structure interaction tool will be useful in studying the coupled mechanics in these grafts towards the reduction and prevention of graft failure. While not conclusive, the initial comparative investigations of arterial and venous anastomotic end-to-side configuration of an upper arm straight PTFE AV access graft indicated a slightly better performance of the 90° arterial and venous end-to-side anastomoses over their counterparts featuring an attachment angle of 135° and 45°, respectively.

ACKNOWLEDGEMENTS

B.D.R. acknowledges the support for the South African Research Chair in Computational Mechanics by the Department of Science and Technology and the National Research Foundation.

APPENDIX

Figures with essential colour discrimination, i.e. Figs. 4 to 8, are difficult to interpret in black and white. The full colour images can be found in the on-line version.

REFERENCES

[1]Aguirre A, Oliva M, Schoephoerster R, Kasyanov V, editors. Static and dynamic mechanical testing of a polymer with potential use as heart valve material. Summer Bioengineering Conference; 2003; Key Biscayne, FL. New York: ASTM; 2003.

[2]B. Braun vascular systems: Vascugraft (http://www.Aesculap-extra.Net/public/frame_doc_index.Html?Med_id=100051022). Berlin: B. Braun Melsungen AG; 2010. p. 8.

[3]Cacho F, Doblare M, Holzapfel GA. A procedure to simulate coronary artery bypass graft surgery. Med Biol Eng Comput. 2007;45(9):819-27.

[4]Chen J, Lu X-Y, Wang W. Non-newtonian effects of blood flow on hemodynamics in distal vascular graft anastomoses. Journal of Biomechanics. 2006;39(11):1983-95.

[5]Cole JS, Watterson JK, O'Reilly MJ. Numerical investigation of the haemodynamics at a patched arterial bypass anastomosis. Med Eng Phys. 2002;24(6):393-401.

[6]Dobrin PB, Littooy FN, Endean ED. Mechanical factors predisposing to intimal hyperplasia and medial thickening in autogenous vein grafts. Surgery. 1989;105(3):393-400.

[7]Ethier CR, Simmons CA. Introductory biomechanics: From cells to organisms. Cambridge texts in biomedical engineering. Cambridge: Cambridge University Press; 2007.

[8]Fisher RK, How TV, Carpenter T, Brennan JA, Harris PL. Optimising miller cuff dimensions. The influence of geometry on anastomotic flow patterns. European Journal of Vascular and Endovascular Surgery. 2001;21(3):251-60.

[9]Garcia-Pajares R, Polo JR, Flores A, Gonzalez-Tabares E, Solis JV. Upper arm polytetrafluoroethylene grafts for dialysis access. Analysis of two different graft sizes: 6 mm and 6–8 mm. Vasc Endovascular Surg. 2003;37(5):335-43.

[10]Gay D, Hoa SV, Tsai SW. Composite materials: Design and applications. Boca Raton: CRC Press; 2003.

[11]Golledge J. Vein grafts: Haemodynamic forces on the endothelium -- a review. Eur J Vasc Endovasc Surg. 1997;14(5):333-43.

[12]Golledge J, Tumer RJ, Harley SL, Springall DR, Powell JT. Development of an in vitro model to study the response of saphenous vein endothelium to pulsatile arterial flow and circumferential deformation. Eur J Vasc Endovasc Surg. 1997;13(6):605-12.

[13]Holzapfel GA, Gasser TC, Ogden RW. A new constitutive framework for arterial wall mechanics and a comparative study of material models. Journal of Elasticity. 2000;61(1-3):1-48.

[14]Kanterman RY, Vesely TM, Pilgram TK, Guy BW, Windus DW, Picus D. Dialysis access grafts: Anatomic location of venous stenosis and results of angioplasty. Radiology. 1995;195(1):135-9.

[15]Kharboutly Z, Deplano V, Bertrand E, Legallais C. Numerical and experimental study of blood flow through a patient-specific arteriovenous fistula used for hemodialysis. Medical Engineering & Physics. 2010;32(2):111-8.

[16]Kharboutly Z, Fenech M, Treutenaere JM, Claude I, Legallais C. Investigations into the relationship between hemodynamics and vascular alterations in an established arteriovenous fistula. Medical Engineering & Physics. 2007;29(9):999-1007.

[17]Kim YH, Chandran KB, Bower TJ, Corson JD. Flow dynamics across end-to-end vascular bypass graft anastomoses. Ann Biomed Eng. 1993;21(4):311-20.

[18]Koch TM, Reddy BD, Zilla P, Franz T. Aortic valve leaflet mechanical properties facilitate diastolic valve function. Computer Methods in Biomechanics and Biomedical Engineering. 2010;13(2):225 - 34.

[19]Kohler T, Kirkman T, Clowes A. The effect of rigid external support on vein graft adaptation to the arterial circulation. J Vasc Surg. 1989;9(2):277-85.

[20]Kundu PK, Cohen IM. Fluid mechanics. 4th ed. Amsterdam: Academic Press; 2008.

[21]Kundu PK, Cohen IM. Fluid mechanics. 4th edition ed. San Diego: Academic Press; 2008.

[22]Lee S-W, Smith DS, Loth F, Fischer PF, Bassiouny HS. Importance of flow division on transition to turbulence within an arteriovenous graft. Journal of Biomechanics. 2007;40(5):981-92.

[23]Lee SW, Fischer PF, Loth F, Royston TJ, Grogan JK, Bassiouny HS. Flow-induced vein-wall vibration in an arteriovenous graft. Journal of Fluids and Structures. 2005;20(6):837-52.

[24]Li L, Terry CM, Shiu YT, Cheung AK. Neointimal hyperplasia associated with synthetic hemodialysis grafts. Kidney Int. 2008;74(10):1247-61.

[25]Li X-M, Rittgers S. Computational simulation of biomechanics in e-PTFE and venous miller's cuffs: Implications for intimal hyperplasia. Journal of Medical Engineering & Technology. 2005;29(4):187 - 96.

[26]Longest PW, Kleinstreuer C. Numerical simulation of wall shear stress conditions and platelet localization in realistic end-to-side arterial anastomoses. J Biomech Eng. 2003;125(5):671-81.

[27]Loth F, Fischer PF, Arslan N, Bertram CD, Lee SE, Royston TJ et al. Transitional flow at the venous anastomosis of an arteriovenous graft: Potential activation of the erk1/2 mechanotransduction pathway. J Biomech Eng. 2003;125(1):49-61.

[28]Malik J, Tuka V, Tesar V. Local hemodynamics of the vascular access for hemodialysis. Kidney Blood Press Res. 2009;32(1):59-66.

[29]Martinez R, Fierro C, Shireman P, Han H-C. Mechanical buckling of veins under internal pressure. Ann Biomed Eng. 2010;38(4):1345-53.

[30]Mitrovic I. Chapter 11. Cardiovascular disorders: Vascular disease. In: McPhee SJ, Hammer GD, editors. Pathophysiology of Disease: An Introduction to Clinical Medicine. 6th ed: McGraw-Hill; 2010.

[31]Morinaga K, Eguchi H, Miyazaki T, Okadome K, Sugimachi K. Development and regression of intimal thickening of arterially transplanted autologous vein grafts in dogs. J Vasc Surg. 1987;5(5):719-30.

[32]O'Callaghan S, Walsh M, McGloughlin T. Numerical modelling of newtonian and non-newtonian representation of blood in a distal end-to-side vascular bypass graft anastomosis. Medical Engineering & Physics. 2006;28(1):70-4.

[33]Ogden RW. Large deformation isotropic elasticity - on the correlation of theory and experiment for incompressible rubberlike solids. Proceedings of the Royal Society of London A Mathematical and Physical Sciences. 1972;326(1567):565-84.

[34]Politis AK, Stavropoulos GP, Christolis MN, Panagopoulos FG, Vlachos NS, Markatos NC. Numerical modeling of simulated blood flow in idealized composite arterial coronary grafts: Steady state simulations. Journal of Biomechanics. 2007;40(5):1125-36.

[35]Porter KE, Nydahl S, Dunlop P, Varty K, Thrush AJ, London NJ. The development of an in vitro flow model of human saphenous vein graft intimal hyperplasia. Cardiovasc Res. 1996;31(4):607-14.

[36]Rhoades RA, Bell DR. Medical physiology: Principles for clinical medicine. 3rd edition ed. Baltimore: Lippincott Williams and Wilkins; 2009.

[37]Schiller NK, Franz T, Weerasekara NS, Zilla P, Reddy BD. A simple fluid–structure coupling algorithm for the study of the anastomotic mechanics of vascular grafts. Computer Methods in Biomechanics and Biomedical Engineering. 2010;13(6):773 - 81.

[38]Schwartz LB, O'Donohoe MK, Purut CM, Mikat EM, Hagen PO, McCann RL. Myointimal thickening in experimental vein grafts is dependent on wall tension. J Vasc Surg. 1992;15(1):176-86.

[39]Su CM, Lee D, Tran-Son-Tay R, Shyy W. Fluid flow structure in arterial bypass anastomosis. J Biomech Eng. 2005;127(4):611-8.

[40]Van Doormaal JP, Raithby GD. Enhancements of the simple method for predicting incompressible fluid flows. Numerical Heat Transfer. 1984;7(2):147 - 63.

[41]Van Tricht I, De Wachter D, Tordoir J, Verdonck P. Hemodynamics and complications encountered with arteriovenous fistulas and grafts as vascular access for hemodialysis: A review. Annals of Biomedical Engineering. 2005;33(9):1142-57.

[42]Van Tricht I, De Wachter D, Tordoir J, Verdonck P. Comparison of the hemodynamics in 6 mm and 4-7 mm hemodialysis grafts by means of CFD. Journal of Biomechanics. 2006;39(2):226-36.

[43]Vazquez MA. Vascular access for dialysis: Recent lessons and new insights. Curr Opin Nephrol Hypertens. 2009;18(2):116-21.

[44]Winsor T, Burch GE. Use of the phlebomanometer: Normal venous pressure values and a study of certain clinical aspects of venous hypertension in man. American Heart Journal. 1946;31(4):387-406.

[45]Zilla P, Wolf M, Rafiee N, Moodley L, Bezuidenhout D, Black M et al. Utilization of shape memory in external vein-graft meshes allows extreme diameter constriction for suppressing intimal hyperplasia: A non-human primate study. Journal of Vascular Surgery. 2009;49(6):1532-42.

[46]Zwolak R, Adams M, Clowes A. Kinetics of vein graft hyperplasia: Association with tangential stress. J Vasc Surg. 1987;5(1):126-36.

TABLES

Table 1: Inner (ID) and outer diameter (OD) assumed for artery, vein and PTFE graft models

	ID (mm)	OD (mm)
PTFE Graft	5.0[2]	6.0*
Artery[30, 20]	4.0	6.0
Vein[20, 30]	5.0	6.0

* Wall thickness WT of approximately 0.5 mm was measured with a vernier caliper on a graft sample; with WT it is OD = ID + 2WT

Table 2: Constitutive parameters of medial and adventitial layers of artery and vein[3], respectively, used in the analyses.

	c (kPa)	k_1 (kPa)	k_2 (-)
Vein media	5.0	36.0	20.0
Vein adventitia	8.0	22.0	19.5
Artery media	7.6	48.0	76.4
Artery adventitia	13.3	265.0	563.0

FIGURES

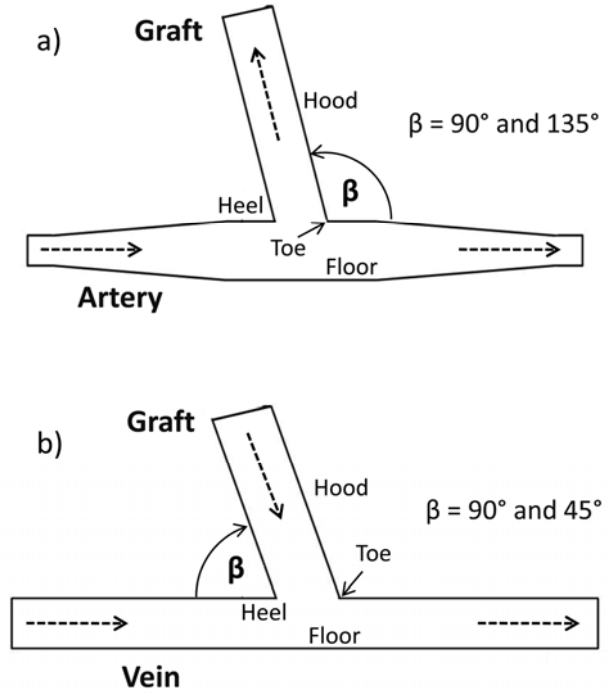

Figure 1: The basic geometries used for a) arterial anastomosis and b) venous anastomosis indicating the attachment angle β and the nomenclature used. Dashed arrows indicate the direction of the blood flow in artery, vein and graft.

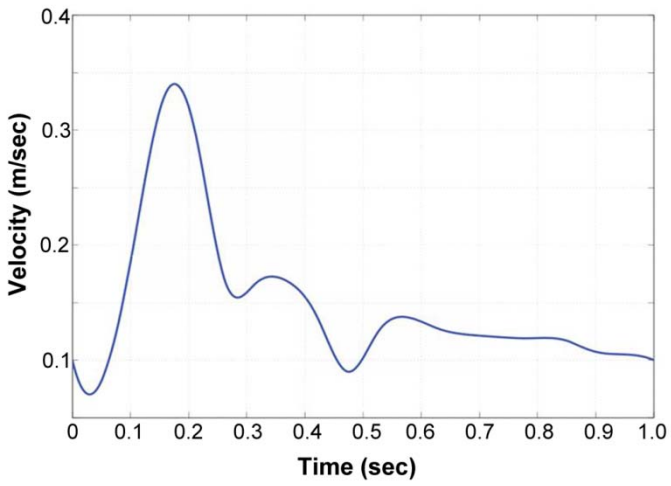

Figure 2: Flow velocity versus time t during one cardiac cycle used for the artery inlet.

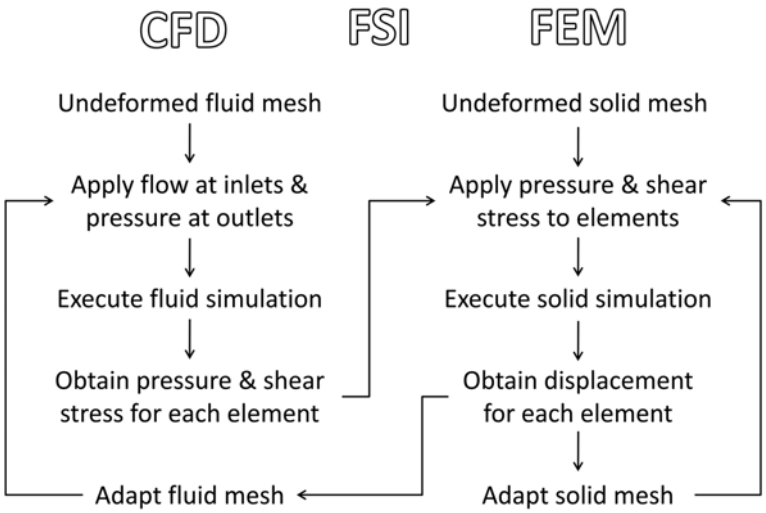

Figure 3: Flow chart illustrating the algorithm used for fluid-structure interaction (FSI) coupling computational fluid dynamics (CFD) simulations with structural simulations using the finite element method (FEM).

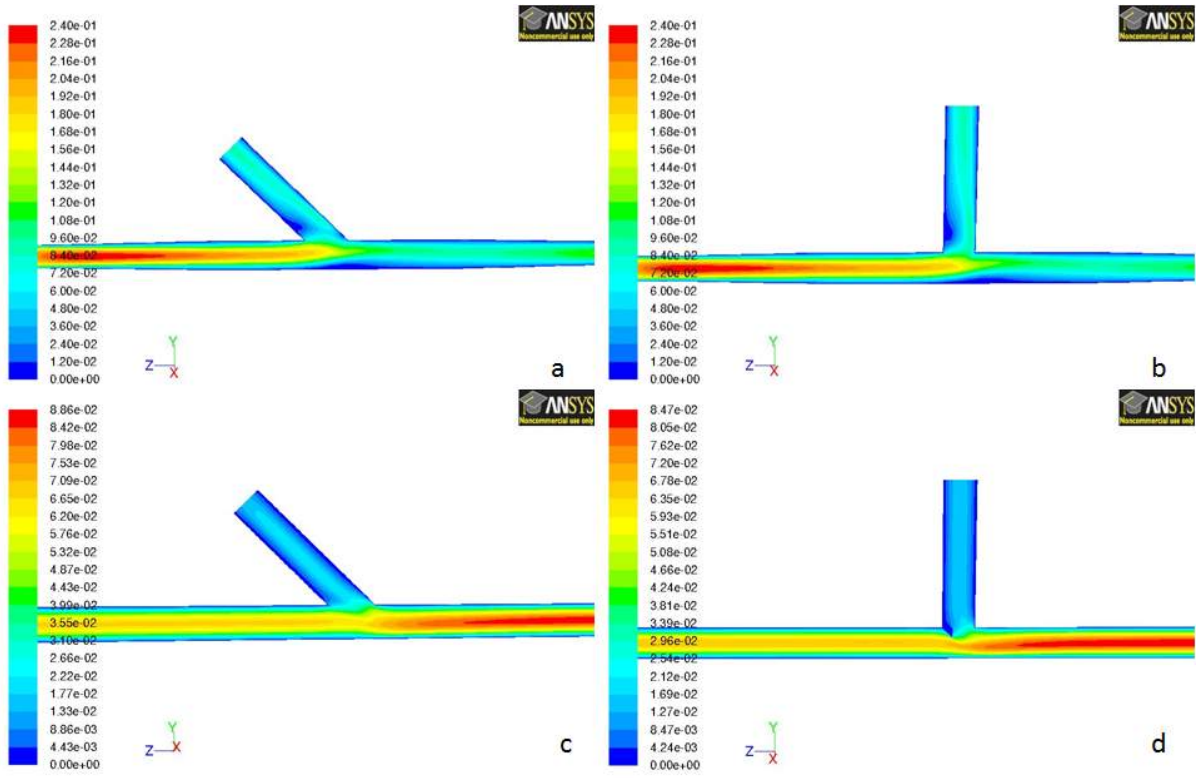

Figure 4: Flow velocity contours at t = 1.0 s for (a) 135° arterial anastomosis, (b) 90° arterial anastomosis, (c) 45° venous anastomosis and (d) 90° venous anastomosis.

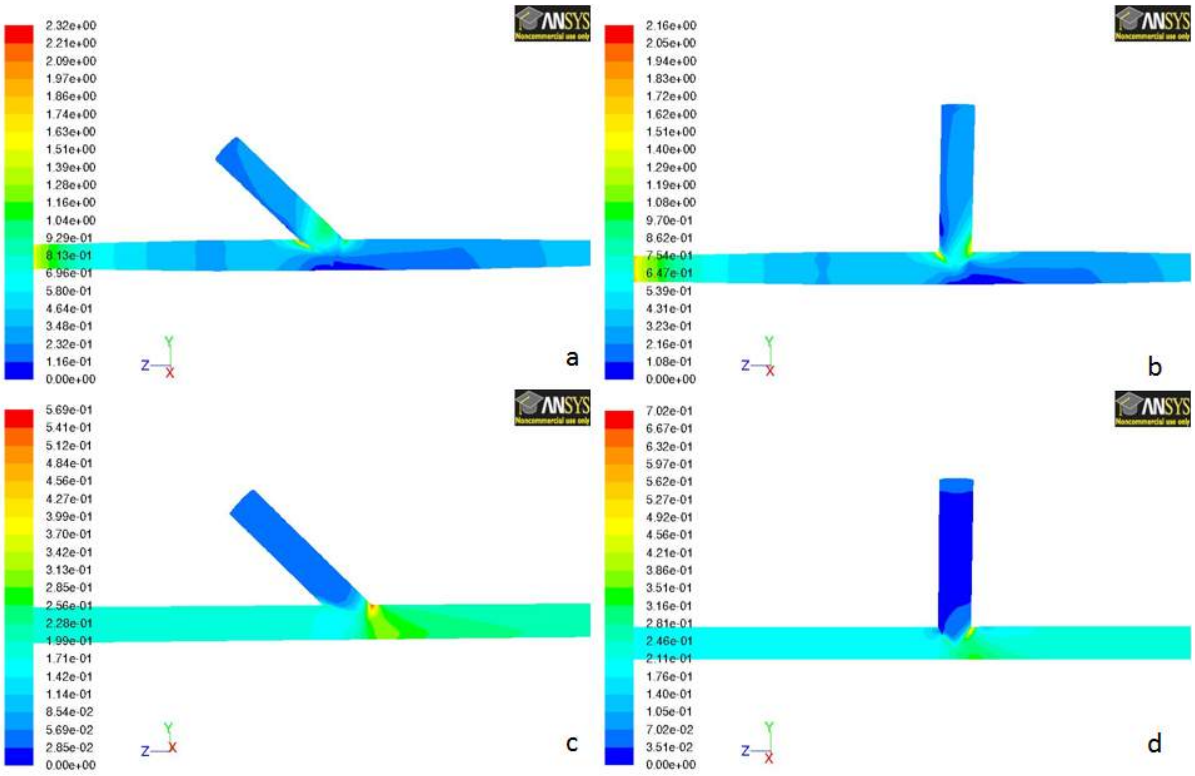

Figure 5: Wall shear stress contours at t = 1.0 s for (a) 135° arterial anastomosis, (b) 90° arterial anastomosis, (c) 45° venous anastomosis and (d) 90° venous anastomosis.

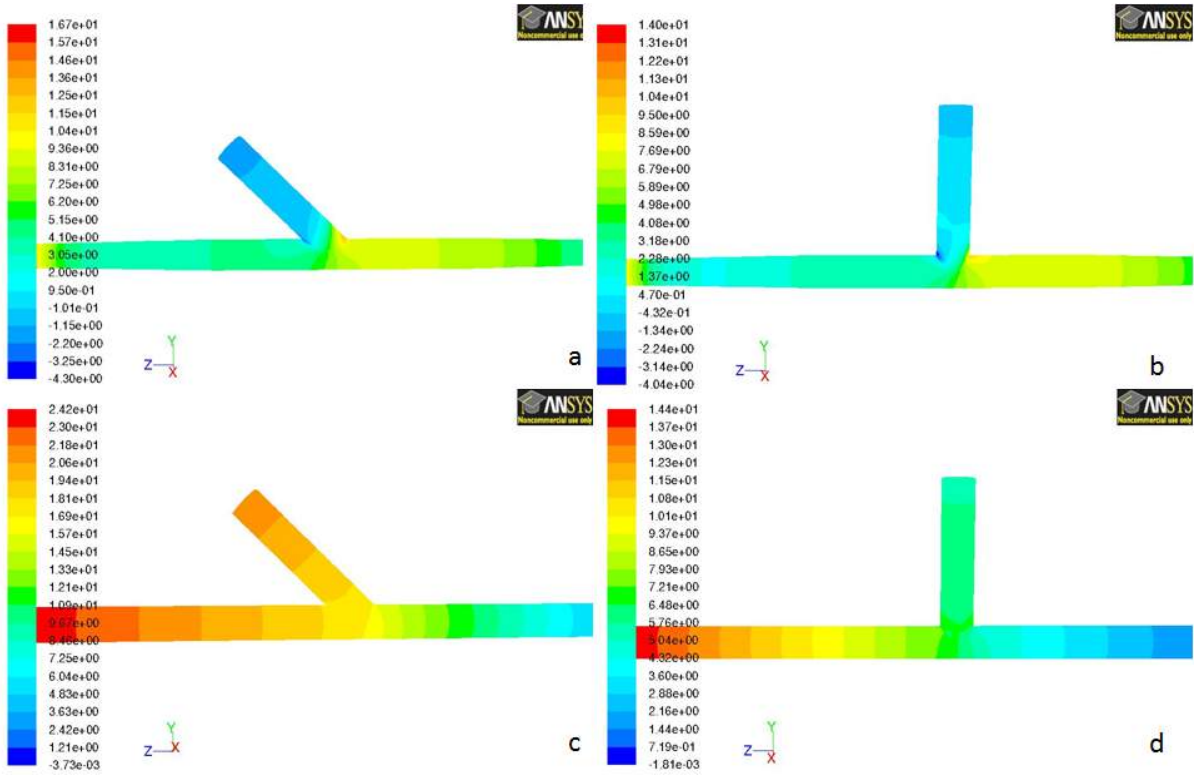

Figure 6: Pressure contours at t = 1.0 s for (a) 135° arterial anastomosis, (b) 90° arterial anastomosis, (c) 45° venous anastomosis and (d) 90° venous anastomosis.

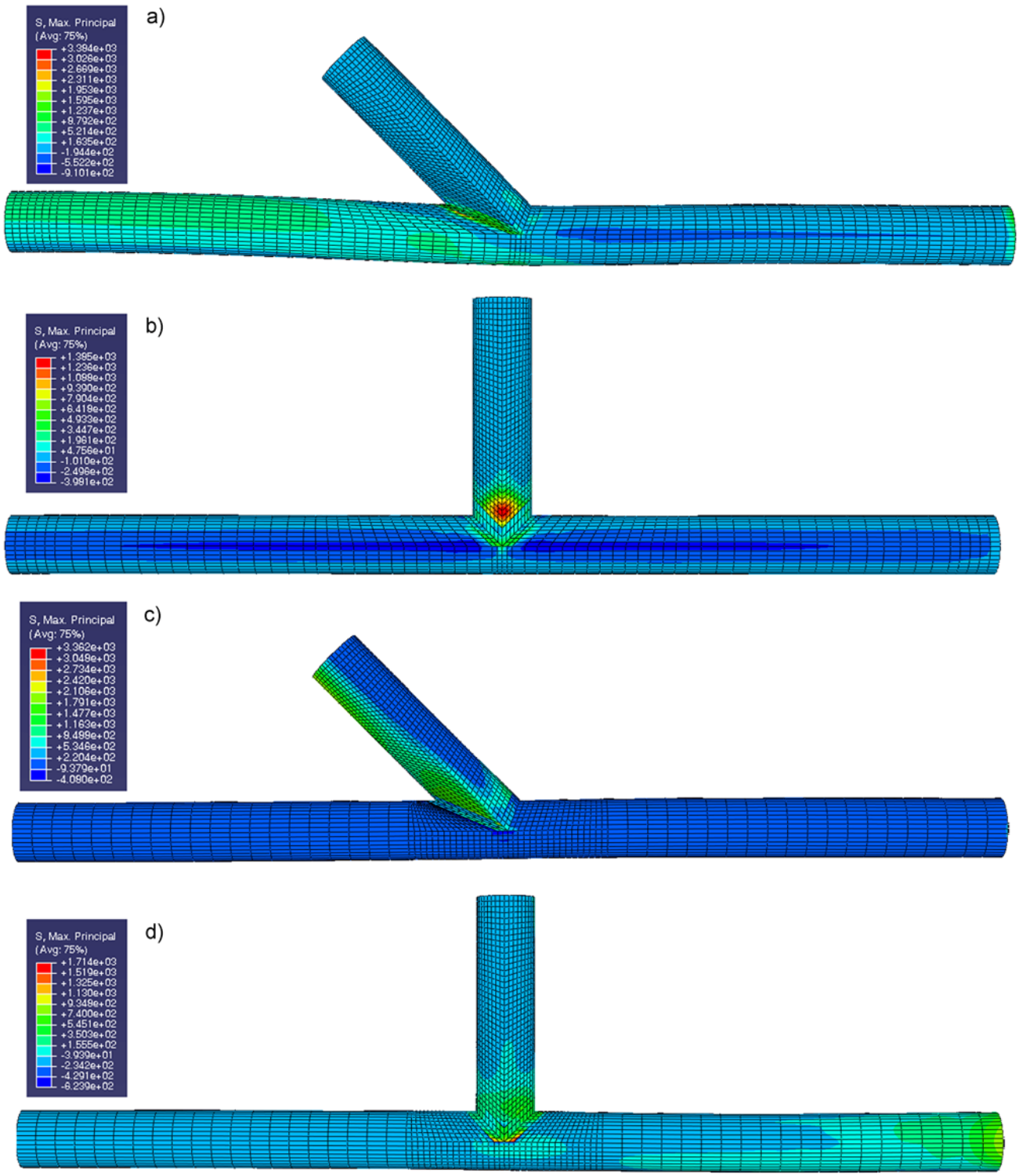

Figure 7: Maximum principal stress contours at t = 1.0 s for (a) 135° arterial anastomosis, (b) 90° arterial anastomosis, (c) 45° venous anastomosis and (d) 90° venous anastomosis.

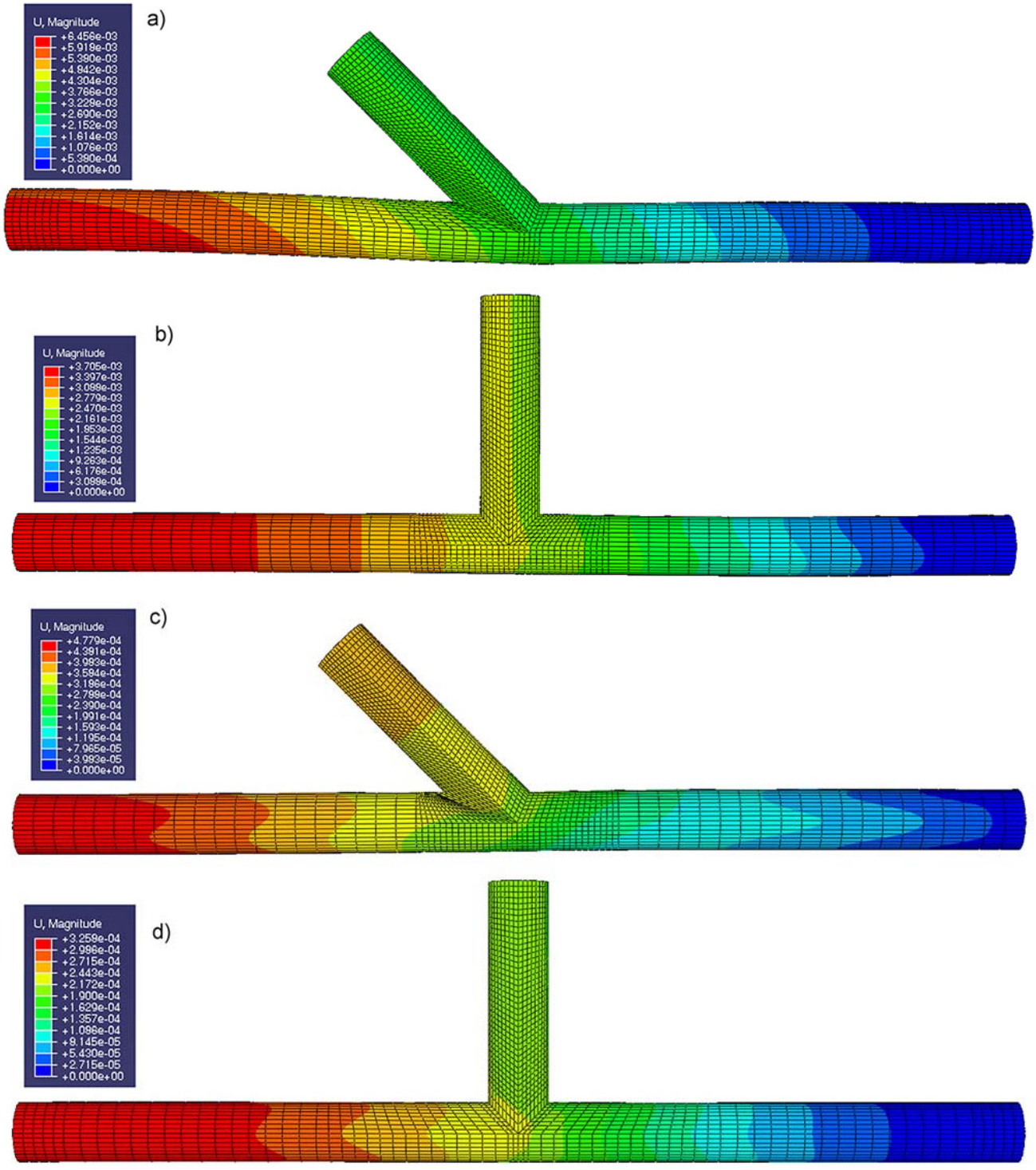

Figure 8: Deformation magnitude contours at t = 1.0 s for (a) 135° arterial anastomosis, (b) 90° arterial anastomosis, (c) 45° venous anastomosis and (d) 90° venous anastomosis.